Fractional order integral sliding mode control for PMSM based on fractional order sliding mode observer

MIAO Zhong-cui, ZHANG Wen-bin, HAN Tian-liang, YU Xian-fei

(*School of Automation and Electrical Engineering, Lanzhou Jiaotong University, Lanzhou 730070, China*)

Abstract: In view of the variation of system parameters and external load disturbance affecting the high-performance control of permanent magnet synchronous motor (PMSM), a fractional order integral sliding mode control (FOISMC) strategy is developed for PMSM drive system by means of fractional order sliding mode observer (FOSMO). Based on FOISMC technology, a fractional order integral sliding mode regulator(FOISM-based regulator) is designed, and a global integral sliding mode surface design method is presented, which can guarantee the global robustness of the system. Combining fractional order theory and sliding mode control theory, the FOSMO is constructed to achieve better identification accuracy of the speed and rotor position. Meanwhile the sliding mode load observer is used to observe the load torque in real time, and the observed value is transmitted to speed regulator to improve the capability of accommodating the challenge of load disturbance. Simulation results validate the feasibility and effectiveness of the proposed scheme.

Key words: fractional order calculus; sliding mode regulator; sliding mode observer; sensorless control; load observer; permanent magnet synchronous motor(PMSM)

CLD number: TM313 **Document code**: A

Article ID: 1674-8042(2019)04-0389-09 **doi**: 10.3969/j.issn.1674-8042.2019.04.011

0 Introduction

Permanent magnet synchronous motor (PMSM) has many advantages such as simple structure, high efficiency and high reliability, therefore it has a wide range of applications in aerospace, new energy vehicles, industrial production and other fields[1-2]. At present, the external loop regulator in the PMSM control system generally adopts proportional intergral (PI) algorithm, which can play a regulatory role within a certain range. However, when the system parameters change or there are external disturbances, the linear regulator is difficult to guarantee the motor to obtain satisfactory performance. In order to improve the robustness of the regulator, modern control theories including fuzzy control, neural network control and sliding mode variable structure control are gradually applied to the high performance control system of the motor[3-8]. Among them, the sliding mode control is widely used in the field of motor control due to its advantages of simple algorithm, good robustness and high reliability[9-11]. However, the output of the traditional sliding mode controller is a high-frequency positive and negative switching value, which brings about the chattering problem of the system. How to reduce the chattering becomes an important direction for the study of sliding mode control. The existing methods mainly include high-order sliding mode control methods and positive lateralization methods within the boundary layer[12]. Although the above method can reduce the chattering to a certain extent, there are still some problems: the high-order sliding mode control algorithm is complex and the chattering phenomenon still exists. After the method of the positive side of the boundary layer is adopted, it is no longer the true sense of sliding modular control[13].

In recent years, with the development of the theory of fractional calculus, some scholars have proposed the fractional sliding mode control theory. Combining the fractional theory with the sliding mode control theory, the use of the fractional-order system with slow decay over time reduces the chattering. In addition, the variability of integral and differential order is increased, which is more robust to the uncertainty of the controlled object model, and

Received date: 2019-05-11

Foundation items: National Natural Science Foundation of China (No. 1461023); Gansu Provincial Education Department Project (No. 2016B-036); Changjiang Scholars and Innovative Research Team (No. RT_16R36)

Corresponding author: ZHANG Wen-bin (745946118@qq.com)

can depict the system characteristics more accurately[14].

Precise acquisition of speed and position information helps improve motor control performance. Sensorless control technology reduces system costs and improves system reliability[15]. In Ref.[16], a model reference adaptive velocity observer is designed for PMSM and good identification accuracy is obtained. However, the essence of this method is linear correction, which is not suitable for the occasion of parameter change or interference. In Ref.[17], an extended Kalman filter is designed for rotor speed and rotor position identification, which has high estimation precision and anti-interference ability. However, the extended Kalman filter algorithm has a large amount of calculation and parameter tuning is difficult. In Refs.[18-20], using high-frequency signal injection method to estimate rotational speed, which has higher observation accuracy and does not require precise motor parameters, but injected high-frequency signals can easily affect the dynamic performance of the system. In this paper, a fractional order sliding mode observer (FOSMO) is designed, which is robust to parameter variations and load disturbance. The variable order gives the observer a unique performance. In order to enhance the robustness of the system, improve the control precision and reduce the cost, the fractional order integral sliding mode control (FOISMC) strategy for PMSM based on fractional order sliding mode observer is proposed. Moreover, the sliding mode load observer is used to observe the load torque in real time, and the observed value is transmitted to speed regulator to improve the capability of accommodating the challenge of load disturbance. Simulation results verify the correctness and effectiveness of the proposed method.

1 Basic theory of fractional calculus

When studying fractional calculus, ${}_aD_t^\alpha$ is generally used to represent the fractional calculus operator, which is expressed as

$$ {}_aD_1^\alpha = \begin{cases} \dfrac{\mathrm{d}^\alpha}{\mathrm{d}t^\alpha} & \mathrm{Re}(\alpha) > 0, \\ 1 & \mathrm{Re}(\alpha) = 0, \\ \displaystyle\int_a^t (\mathrm{d}t)^{-\alpha} & \mathrm{Re}(\alpha) < 0. \end{cases} \tag{1} $$

Fractional order calculus has the following properties[20-21]:

1) When $\alpha = 0$, ${}_aD_t^\alpha f(t) = f(t)$; When $\alpha = 1$, ${}_aD_t^\alpha f(t) = \mathrm{d}f(t)/\mathrm{d}t$;

2) The commutative law is applied to fractional calculus and then a superposition relationship is expressed as

$$ {}_aD_t^\alpha [{}_aD_t^\beta f(t)] = {}_aD_t^\beta [{}_aD_t^\alpha f(t)] = {}_aD_t^{\alpha+\beta} f(t). $$

In this paper, the fractional calculus operator is implemented using the improved Oustaloup filter algorithm[22]; ${}_aD_t^\alpha$ is replaced by the symbol D^α for convenience.

2 Design of fractional-order integral sliding mode speed regulator

In this paper, surface mounted PMSM ($L_s = L_d = L_q$) is taken as the control object, hysteresis and eddy current loss are not taken into account; the saturation of the motor core is ignored; assuming that the space magnetic field is sinusoidal. The voltage equation in rotor synchronous reference frame (dq-frame) is expressed as

$$ \begin{cases} u_d = Ri_d + L_s \dfrac{\mathrm{d}i_d}{\mathrm{d}t} - p\omega_m L_s i_q, \\ u_q = Ri_q + L_s \dfrac{\mathrm{d}i_q}{\mathrm{d}t} + p\omega_m L_s i_q + p\omega_m \psi_f, \end{cases} \tag{2} $$

where u_d and u_q are stator voltages, i_d and i_q are stator currents, L_s is stator inductance, ω_m is rotor mechanical angular velocity, p and ψ_f are polar logarithm and permanent magnet flux linkage, respectively.

The field oriented control strategy of $i_d = 0$ is adopted, and the equation of rotor mechanical motion is expressed as

$$ J \frac{\mathrm{d}\omega_m}{\mathrm{d}t} = \frac{3}{2} p\psi_f i_q - T_L - B\omega_m, \tag{3} $$

where J is the moment of inertia, T_L is the load torque, and B is the damping factor.

2.1 Design of fractional order integral sliding mode surface

The design objective of the speed regulator is to make the actual speed ω_m follow the given speed ω_m^* quickly and accurately, and the speed error is defined as

$$ e(t) = \omega_m^* - \omega_m. \tag{4} $$

Fractional order integral sliding mode (FOISM) surface is designed as

$$ s = e(t) + c_1 D^{-u} e(t), \tag{5} $$

where $c_1>0$ is the integral constant; $0<u<1$ is the fractional order sliding mode surface order.

In the sliding mode variable structure control, the system state point has two stages of movement: one is the forward movement from the arbitrary state to the sliding mode area; the other is the sliding mode movement after reaching the sliding mode area. Sliding mode control does not guarantee the robustness of the first stage. In order to make the system globally robust, the fractional integral sliding mode surface is designed as

$$s = e(t) + c_1 D^{-u} e(t) + h(t), \tag{6}$$

where $h(t)=h(0)\exp\left(-\frac{t}{n}\right)$, $n>0$ and n determines the convergence rate of $h(t)$; $h(0)=-e(0)-c_1\times {}_0D_0^{-u}e(0)$, $e(0)$ is the initial value of the error, and ${}_0D_0^{-u}e(0)$ is the fractional integral value at time $t=0$. When $t=0$, the initial state is $s=0$, that is, the initial state of the system is located on the sliding surface, which eliminates the arrival process and makes the system globally robust. In addition, the integral function can also eliminate the steady-state error of the system.

2.2 Design of the regulator

Let $m=h(0)$, it can be observed from Eq. (6) as

$$s = e(t) + c_1 D^{-u} e(t) + m\exp\left(-\frac{t}{n}\right), \tag{7}$$

then

$$\dot{s} = \dot{e}(t) + c_1 D^{1-u} e(t) - \frac{m}{n}\exp\left(-\frac{t}{n}\right). \tag{8}$$

Selecting the isokinetic reaching law

$$\dot{s} = -\varepsilon \mathrm{sgn}(s),\ \varepsilon > 0, \tag{9}$$

and combining Eqs. (3), (4), (8) and (9), the output of the speed regulator can be deduced as

$$i_q = \frac{2J}{3p\psi_f}\left[\dot{\omega}_m^* + c_1 D^{1-u} e(t) - \frac{m}{n}\exp\left(-\frac{t}{n}\right) + \frac{T_L}{J} + \frac{B\omega_m}{J} + \varepsilon \mathrm{sgn}(s)\right]. \tag{10}$$

In order to weaken the high-frequency buffeting phenomenon in the traditional sliding mode control and make the speed error converge to the sliding surface quickly, we introduce a new approach law, inverse hyperbolic sine function arsh (•). The sliding mode approach law is designed as

$$\dot{s} = -\eta \mathrm{arsh}(s), \tag{11}$$

where $\eta>0$ is the sliding mode gain; arsh(•) is an inverse hyperbolic sine function, which is an approximate linear function near the origin, and can be used to smooth and limit amplitude while accelerating the state to approach the sliding mode surface and reduce system chattering. This feature is not available with the traditional symbol function sgn(•) or the saturation function sat(•).

From Eqs. (10) and (11), the output of the regulator with inverse hyperbolic sine function is expressed as

$$i_q = \frac{2J}{3p\psi_f}\left[\dot{\omega}_m^* + c_1 D^{1-u} e(t) - \frac{m}{n}\exp\left(-\frac{t}{n}\right) + \frac{T_1}{J} + \frac{B\omega_m}{J} + \eta \mathrm{arsh}(s)\right]. \tag{12}$$

2.3 Stability analysis of FOISM-based regulator

To verify the stability of the designed speed regulator, the Lyapunov function is constructed as

$$V_1 = \frac{1}{2}s^2. \tag{13}$$

According to the Lyapunov stability theorem, when $\dot{V}_1 = s\dot{s}<0$, the system satisfies the stability condition.

According to Eqs. (7), (8), (12) and (13), we can obtain

$$\begin{aligned}
\dot{V}_1 = s\dot{s} &= s\left[D^{1-u}D^u s\right] = \\
&s\left[\dot{e}(t) + c_1 D^{1-u} e(t) + \dot{h}(t)\right] = \\
&s\left[\dot{e}(t) + c_1 D^{1-u} e(t) - \frac{m}{n}\exp\left(-\frac{t}{n}\right)\right] = \\
&s\left[\dot{\omega}_m^* - \frac{1}{J}\left(\frac{3}{2}p_n\psi_f i_q - T_L - B\omega_m\right) + c_1 D^{1-u} e(t) - \frac{m}{n}\exp\left(-\frac{t}{n}\right)\right] = \\
&s\left[-\eta \mathrm{arsh}(s)\right] = -\eta\,|\,s\,|.
\end{aligned} \tag{14}$$

When $\eta>0$ and $\dot{V}_1<0$, the Lyapunov stability theory is satisfied, therefore the designed FOISM-based regulator is stable and its movement can tend to sliding mode surface and finally reach the sliding mode.

3 Design of FOSMO mode observer

3.1 Design of stator current and back EMF FOSMO

The current state equation of PMSM in two-phase

stationary reference frame ($\alpha\beta$-frame) is expressed as

$$\begin{cases} \dfrac{\mathrm{d}i_\alpha}{\mathrm{d}t} = -\dfrac{R_s}{L_s}i_\alpha + \dfrac{1}{L_s}u_\alpha + \dfrac{1}{L_s}\psi_f\omega_e\sin\theta, \\ \dfrac{\mathrm{d}i_\beta}{\mathrm{d}t} = -\dfrac{R_s}{L_s}i_\beta + \dfrac{1}{L_s}u_\beta - \dfrac{1}{L_s}\psi_f\omega\mathrm{e}\cos\theta. \end{cases} \tag{15}$$

Back electromotive fore (EMF) equation is expressed as

$$\begin{bmatrix} E_\alpha \\ E_\beta \end{bmatrix} = \begin{bmatrix} -\psi_f\omega_e\sin\theta \\ \psi_f\omega_e\cos\theta \end{bmatrix}. \tag{16}$$

Observing Eqs. (15) and (16), we can see that there is a coupling term between the stator current equation and the back EMF equation. Using the functions h_α and h_β instead of the coupling term, the current and back EMF observation equations can be obtained as

$$\begin{bmatrix} \dfrac{\mathrm{d}\hat{i}_\alpha}{\mathrm{d}t} \\ \dfrac{\mathrm{d}\hat{i}_\beta}{\mathrm{d}t} \end{bmatrix} = -k_1\begin{bmatrix} \hat{i}_\alpha \\ \hat{i}_\beta \end{bmatrix} + k_2\begin{bmatrix} h_\alpha \\ h_\beta \end{bmatrix} + k_2\begin{bmatrix} u_\alpha \\ u_\beta \end{bmatrix}, \tag{17}$$

$$\begin{bmatrix} \hat{E}_\alpha \\ \hat{E}_\beta \end{bmatrix} = -\begin{bmatrix} h_\alpha \\ h_\beta \end{bmatrix}, \tag{18}$$

where

$$k_1 = \frac{R_s}{L_s},\ k_2 = \frac{1}{L_s},\ \text{and}\ \begin{bmatrix} h_\alpha \\ h_\beta \end{bmatrix} = \begin{bmatrix} \psi_f\omega_e\sin\theta \\ -\psi_f\omega_e\cos\theta \end{bmatrix}. \tag{19}$$

The sliding surface of the FOSMO is defined as

$$s = \begin{bmatrix} s_\alpha \\ s_\beta \end{bmatrix} = \begin{bmatrix} \lambda_1\tilde{i}_\alpha + \lambda_2 D^{-u}\tilde{i}_\alpha \\ \lambda_1\tilde{i}_\beta + \lambda_2 D^{-u}\tilde{i}_\beta \end{bmatrix}, \tag{20}$$

where $\hat{i}_\alpha$ and $\hat{i}_\beta$ are observed values of the stator current in $\alpha\beta$-frame; i_α and i_β are the actual current values; $\begin{cases} \tilde{i}_\alpha = \hat{i}_\alpha - i_\alpha \\ \tilde{i}_\beta = \hat{i}_\beta - i_\beta \end{cases}$, $\tilde{i}_\alpha$ and $\tilde{i}_\beta$ are the observation errors of the stator current; D^{-u} is the fractional integral operator; $\lambda_1 \in \mathbf{R}^+$, $\lambda_2 \in \mathbf{R}^+$, $u \in (0,1]$.

According to Eqs. (19) and (20), taking the first-order derivative of s, we can obtain

$$\dot{s} = \lambda_1\begin{bmatrix} \dot{\tilde{i}}_\alpha - \dot{i}_\alpha \\ \dot{\tilde{i}}_\beta - \dot{i}_\beta \end{bmatrix} + \lambda_2 D^{1-u}\begin{bmatrix} \tilde{i}_\alpha \\ \tilde{i}_\beta \end{bmatrix} = \lambda_1 k_2\begin{bmatrix} h_\alpha \\ h_\beta \end{bmatrix} + \lambda_1 k_2\begin{bmatrix} M \\ R \end{bmatrix} - \lambda_1 k_1\begin{bmatrix} \tilde{i}_\alpha \\ \tilde{i}_\beta \end{bmatrix} + \lambda_2 D^{1-u}\begin{bmatrix} \tilde{i}_\alpha \\ \tilde{i}_\beta \end{bmatrix}, \tag{21}$$

where $M = -\psi_f\omega_e\sin\theta$, $R = \psi_f\omega_e\cos\theta$.

Defining Lyapunov function as

$$V_2 = \frac{1}{2}s^{\mathrm{T}}s, \tag{22}$$

and differentiating Eq. (22), there is

$$\dot{V}_2 = \dot{s}s^{\mathrm{T}}\left\{\lambda_1 k_2\begin{bmatrix} h_\alpha \\ h_\beta \end{bmatrix} + \lambda_1 k_2\begin{bmatrix} M \\ R \end{bmatrix} - \lambda_1 k_1\begin{bmatrix} \tilde{i}_\alpha \\ \tilde{i}_\beta \end{bmatrix} + \lambda_2 D^{1-u}\begin{bmatrix} \tilde{i}_\alpha \\ \tilde{i}_\beta \end{bmatrix}\right\}. \tag{23}$$

Supposing that

$$\max|\lambda_1 k_2 M| < M\alpha < +\infty,$$
$$\max|\lambda_1 k_2 R| < M_\beta < +\infty,$$

that is, $s_\alpha\max|\lambda_1 k_2 M| < M_\alpha s_\alpha\mathrm{sgn}(s_\alpha)$, $s_\beta\max|\lambda_1 k_2 R| < M_\beta s_\beta\mathrm{sgn}(s_\beta)$, thus Eq. (23) can be expressed as

$$\dot{V} < s^{\mathrm{T}}\left\{\lambda_1 k_2\begin{bmatrix} h_\alpha \\ h_\beta \end{bmatrix} + \begin{bmatrix} \mathrm{sgn}(s_\alpha)M_\alpha \\ \mathrm{sgn}(s_\beta)M_\beta \end{bmatrix} - \lambda_1 k_1\begin{bmatrix} \tilde{i}_\alpha \\ \tilde{i}_\beta \end{bmatrix} + \lambda_2 D^{1-u}\begin{bmatrix} \tilde{i}_\alpha \\ \tilde{i}_\beta \end{bmatrix}\right\}. \tag{24}$$

Under the condition of Lyapunov stability, according to Eq. (24), the stable fractional order sliding mode control law is deduced as

$$\begin{bmatrix} h_\alpha \\ h_\beta \end{bmatrix} = \frac{k_1}{k_2}\begin{bmatrix} \tilde{i}_\alpha \\ \tilde{i}_\beta \end{bmatrix} - \frac{u_0}{\lambda_1 k_2}\begin{bmatrix} \mathrm{sgn}(s_\alpha) \\ \mathrm{sgn}(s_\beta) \end{bmatrix} - \frac{\lambda_2 D^{1-u}}{\lambda_1 k_2}\begin{bmatrix} \tilde{i}_\alpha \\ \tilde{i}_\beta \end{bmatrix}, \tag{25}$$

where $u_0 \in \mathbf{R}^+$, $\mathrm{sgn}(s)$ is the sign function, described as

$$\mathrm{sgn}(s) = \begin{cases} 1 & s > 0, \\ -1 & s < 0. \end{cases} \tag{26}$$

To prove the accessibility of the sliding surface, assuming that $u_0 > \max(M_\alpha, M_\beta)$, and substituting Eq. (25) for Eq. (24), we can obtain

$$\dot{V} \leqslant \begin{bmatrix} s_\alpha \\ s_\beta \end{bmatrix}\left\{-\begin{bmatrix} u_0\mathrm{sgn}(s_\alpha) \\ u_0\mathrm{sgn}(s_\beta) \end{bmatrix} + \begin{bmatrix} \mathrm{sgn}(s_\alpha)M_\alpha \\ \mathrm{sgn}(s_\beta)M_\beta \end{bmatrix}\right\} = s_\alpha\mathrm{sgn}(s_\alpha)(u_0 - M_\alpha) + s_\beta\mathrm{sgn}(s_\beta)(u_0 - M_\beta). \tag{27}$$

Then $\dot{V} < 0$, that is, the sliding surface is reachable, and the designed FOSMO observer gradually converges.

From Eq. (19), it can be seen that the sign function is involved, therefore the chattering phenomenon will be caused. Correspondingly, a power function is adopted to reduce the chattering problem, namely

$$\mathrm{fal}(s,\varepsilon,\delta) = \begin{cases} \dfrac{s}{\delta^{1-\varepsilon}}, & |s| \leqslant \delta, \\ \mathrm{sgn}(s)\,|s|^{\varepsilon}, & |s| > \delta, \end{cases} \tag{28}$$

where $\delta > 0$ is the filter factor, $0 < \varepsilon < 1$ is the non-linear factor, and fal(·) is the linear function near the equilibrium point (origin), which has the

characteristics of large gain and small error.

According to Eqs. (25) and (28), the fractional-order sliding mode control law using a new power function can be deduced as

$$\begin{bmatrix} h_\alpha \\ h_\beta \end{bmatrix} = \frac{k_1}{k_2}\begin{bmatrix} \tilde{i}_\alpha \\ \tilde{i}_\beta \end{bmatrix} - \frac{u_0}{\lambda_1 k_2}\begin{bmatrix} \mathrm{fal}(s_\alpha) \\ \mathrm{fal}(s_\beta) \end{bmatrix} - \frac{\lambda_2 D^{1-u}}{\lambda_1 k_2}\begin{bmatrix} \tilde{i}_\alpha \\ \tilde{i}_\beta \end{bmatrix}. \tag{29}$$

Substituting Eq. (29) into Eqs. (18) and (19), the observed values of stator current and back EMF can be obtained.

3.2 Estimation of speed and rotor position

For the surface mounted PMSM, the electromagnetic angular velocity ω_e can be directly calculated from the back-EMF observations. The expression is

$$\hat{\omega}_e = \frac{\sqrt{\hat{E}_\alpha^2 + \hat{E}_\beta^2}}{\psi_f}. \tag{30}$$

The rotor position can be obtained by the inverse tangent function method, which is

$$\theta_e = -\arctan\frac{\hat{E}_\alpha}{\hat{E}_\beta}. \tag{31}$$

4 Design of load torque observer

Combined with the motor mechanical motion Eq. (3), the rotor mechanical angular velocity ω_m and load torque T_L are taken as state variables; the state equation of PMSM is constructed as

$$\begin{cases} \dfrac{\mathrm{d}\omega_m}{\mathrm{d}t} = \dfrac{3p\psi_f}{2J} i_q - \dfrac{T_L}{J} - \dfrac{B}{J}\omega_m, \\ \dot{T}_L = 0. \end{cases} \tag{32}$$

Based on Eq. (3), the sliding mode observation equations for rotor mechanical angular velocity and load torque are constructed as

$$\begin{cases} \dfrac{\mathrm{d}\hat{\omega}_m}{\mathrm{d}t} = \dfrac{3p\psi_f}{2J} i_q - \dfrac{\hat{T}_L}{J} - \dfrac{B}{J}\hat{\omega}_m + U, \\ \dot{\hat{T}}_L = gU, \end{cases} \tag{33}$$

where $U = k\,\mathrm{sat}(\hat{\omega}_m - \omega_m)$, $\mathrm{sat}(\cdot)$ is the saturation function, k is the sliding mode gain, and g is the feedback gain. Subtracting Eq. (33) from Eq. (32) gives the sliding mode observation error equation as

$$\begin{cases} \dot{e}_1 = -\dfrac{e_2}{J} - \dfrac{B}{J}e_1 + U, \\ \dot{e}_2 = gU, \end{cases} \tag{34}$$

where $e_1 = \hat{\omega}_m - \omega_m$ is the observation error of the speed, $e_2 = \hat{T}_L - T_L$ is the observation error of the load torque. The sliding surface function is defined as

$$s = e_1 - \hat{\omega}_m - \omega_m. \tag{35}$$

In order to make the sliding mode of the observer exist and stable, the Lyapunov function $V = \frac{1}{2}s^2$ is constructed. To satisfy $s\dot{s} \leqslant 0$, that is

$$s\dot{s} = e_1\left[k\,\mathrm{sat}(e_1) - \frac{e_2}{J} - \frac{B}{J}e_1\right] \leqslant 0, \tag{36}$$

we can deduce the range of sliding mode gain as $k \leqslant -\left|\dfrac{Be_1 + e_2}{J}\right|$. After the sliding mode observer entering the sliding mode, $s = \dot{s} = 0$, that is, $e_1 = \dot{e}_1 = 0$, Eq. (34) can be expressed as

$$\begin{cases} U = \dfrac{e_2}{J}, \\ \dot{e}_2 = gU. \end{cases} \tag{37}$$

Furthermore, we can simplify Eq. (37) to obtain the error state equation of load torque as

$$\dot{e}_2 - g\frac{e_2}{J} = 0. \tag{38}$$

According to stability theory, the stable condition of the system is $-\dfrac{g}{J} < 0$, that is, $g < 0$. Selecting load observer parameters reasonably can ensure the stability of the observer and estimate the value of load torque. The structure diagram of the load torque observer is shown in Fig. 1.

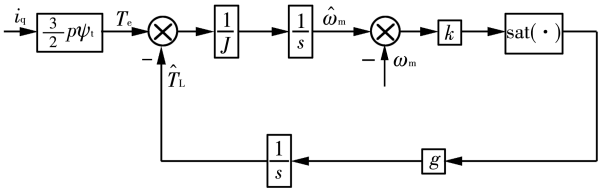

Fig. 1 Structure diagram of load torque observer

Substituting the load observations obtained by the load observer into Eq. (12), then Eq. (12) can be rewritten as

$$i_q = \frac{2J}{3p\psi_f}\left[\dot{\omega}_m^* + c_1 D^{1-u}e(t) - \frac{m}{n}\exp\left(-\frac{t}{n}\right) + \frac{\hat{T}_L}{J} + \frac{B\omega_m}{J} + \eta\,\mathrm{arsh}(s)\right]. \tag{39}$$

From Eq. (39), it can be seen that the observed load torque is fed back to the speed regulator. When the load is disturbed, the regulator can respond to the change of the load in time and reduce the influence of the load disturbance on the control performance.

5 Simulation and analysis

In order to verify the effectiveness of the proposed control strategy, the designed control system has been implemented in Matlab/Simulink platform. The block diagram of the control system is shown in Fig. 2.

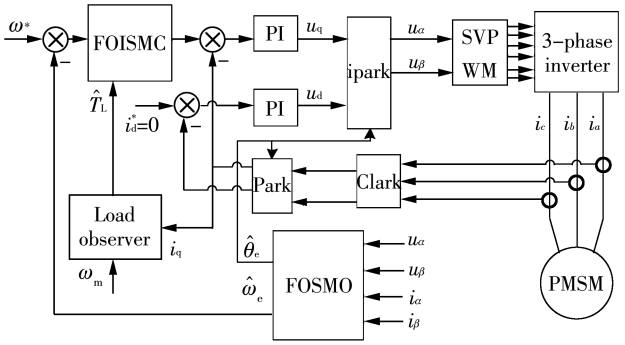

Fig. 2 Block diagram of PMSM control system

The parameters in the PMSM drive system are listed in Table 1.

Table 1 Parameters of PMSM

Parameters	Values
DC bus voltage U_{dc}	300 V
Rated torque T_N	3 N·m
Number of poles p	2
Phase resistance R_s	2.875 Ω
Rotor flux ψ_f	0.175 Wb
Stator inductance L_s	0.008 5 H
Motor inertia J	0.000 8 kg·m^2
Friction coefficient B	0.001 N·m·s

1) Speed regulator simulation comparison

The PI-based regulator and the integer-order integral sliding mode regulator (IOISM-based regulator) are constructed, respectively, and then compared with the FOISM-based regulator designed. In simulation, the parameters of the PI-based regulator are $k_p=11$ and $k_i=0.1$; the parameters of the IOISM-based regulator are $c_1=475$, $n=22$, $\eta=9$ and $u=1$; the parameter of the FOISM-based regulator is $u=0.8$.

2) Speed observer simulation comparison

The model reference adaptive observer (MRAS) and the integer order sliding mode observer (SMO) are constructed, respectively, and then compared with the FOSMO designed. In simulation, the parameters of the FOSMO are $\lambda_1=0.003\ 5$, $\lambda_2=1.2$, $\varepsilon=0.38$, $\beta=0.01$, $u_0=11\ 000$ and $u=0.5$.

3) Load observer simulation comparison

A load torque observer using the direct calculation method (DCM-based observer) is constructed and compared with the sliding mode load observer (SMO-based observer) proposed. The parameters of the SMO-based observer are $k=-1\ 500$ and $g=-0.8$.

5.1 Comparison of speed regulator performance

For the FOISM surface designed, the simulation parameters above are used to obtain the simulation curve of the sliding surface function s, as shown in Fig. 3.

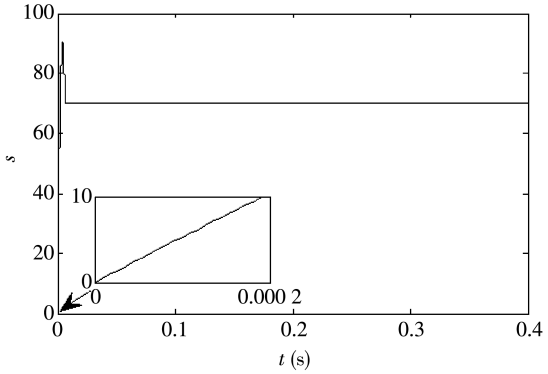

Fig. 3 Simulation curve of sliding surface function s

Since $e(t)=\omega_m^*-\omega_m$ is a positive value during the start-up stage, so $s=e(t)+c_1D^{-u}e(t)+h(t)$ shows an upward trend in Fig. 3. Meanwhile, because $h(t)$ is set in the function of s, the initial value of s is 0, that is, the initial state of the system is on the sliding surface. When the actual speed is tracked on given speed, the speed error $e(t)=0$. Since the integral term D^{-u} exists in the function of s, the value of function s is stabilized near a constant value.

For the purpose of validating the robustness of the FOISM-based regulator to load disturbance, a comparative simulation experiment was conducted for the motor with load start (1 N·m), given speed of 1 000 r/min, and increased load to rated load (3 N·m) at 0.1 s. Fig. 4 shows the dynamic response comparison curves for the three speed regulators.

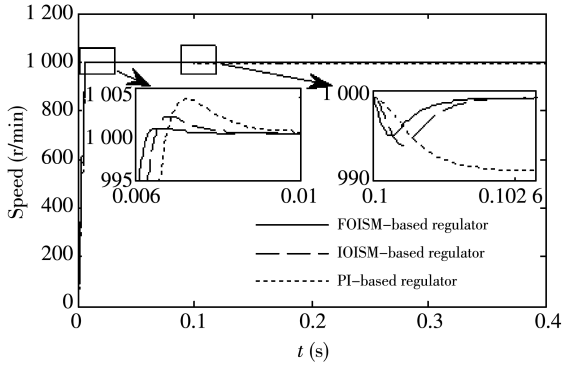

Fig. 4 Rotor speed response

It can be seen from Fig. 4 that compared with the systems using PI-based regulator and IOISM-based regulator, the system using FOISM-based regulator possesses better transient response characteristics, that is, it has smaller overshoot as well as adjusting time. After increasing the load to the rated value at 0.1 s, the system using the FOISM-based regulator shows better robustness against load disturbance, namely, lower speed drop and faster load recovery.

5.2 Comparison of speed observation methods

In order to test and prove the estimation accuracy of the FOSMO, a comparative experiment was carried out with the star-tup load of 1 N · m and the rated load of 3 N · m at 0.1 s. Fig. 5 and Fig. 7 illustrate the comparison of the speed and rotor position estimations of the three observers, respectively. Fig. 6 and Fig. 8 have expressed the speed estimation error and the rotor position estimation error, respectively.

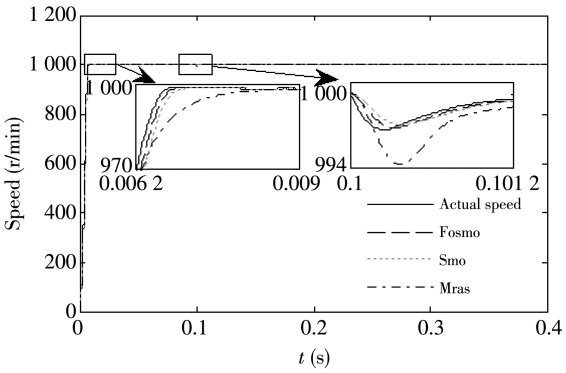

Fig. 5 Estimated speed

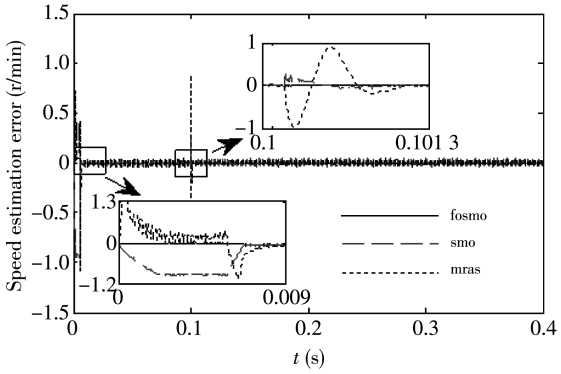

Fig. 6 Error of estimated speed

Fig. 5 shows speed tracking comparison curves of the three observers. Compared with the other two observers, the FOSMO can more accurately follow the actual speed both in the case of load start-up and increase to the rated load. Moreover, Fig. 6 also shows that the estimated speed error of the FOSMO fluctuates slightly at the moment of sudden load change, but decreases quickly under the control law, and the observed speed tracks the actual speed fast and accurately. Figs. 7 and 8 intuitively demonstrate that the FOSMO has higher estimation accuracy and stronger robustness to load disturbance than the others.

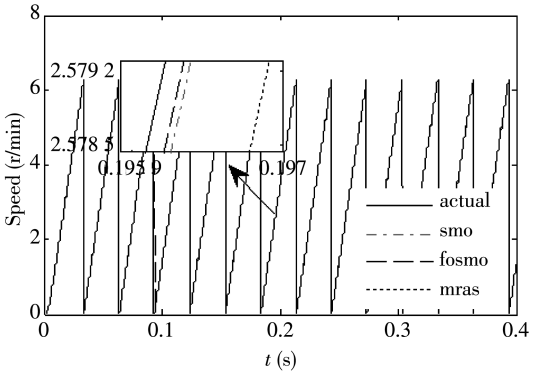

Fig. 7 Estimated rotor position

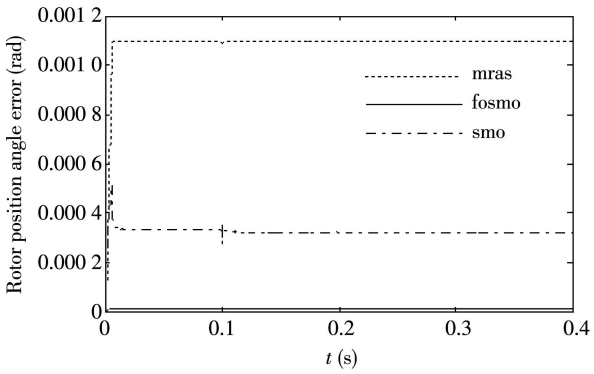

Fig. 8 Error of estimated rotor position

5.3 Comparison of load torque identification methods

To verify the performance of the designed load observer, first the motor is loaded (1 N · m) to start, then loaded to the rated load (3 N · m) at 0.1 s, finally suddenly reduced to 2 N · m at 0.2 s. The tracking performance of two load observers as well as the influence of load observers on speed response are compared. Fig. 9 shows the curves of two load observers for actual load. Fig. 10 shows the influence of load observer on speed response.

From Fig. 9, it can be observed that the sliding mode load observer proposed tracks the actual load torque quickly and accurately, which is faster than the direct calculation method. Meanwhile, it can be seen from Fig. 10 that when there is load disturbance, the system adopting the sliding mode load observer has less fluctuation speed and can

restore to reference speed faster. It can be found that the sliding mode load observer can overcome the influence of load disturbance effectively as well as improve the robustness of the system significantly.

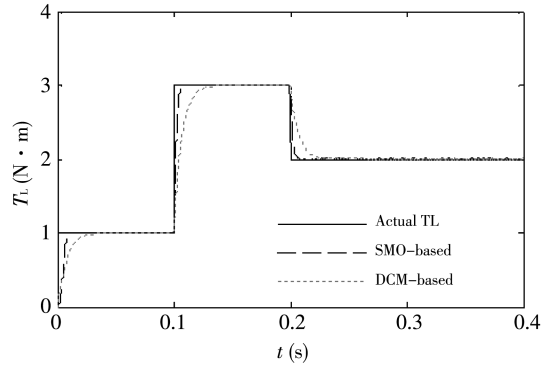

Fig. 9 Estimated load torque

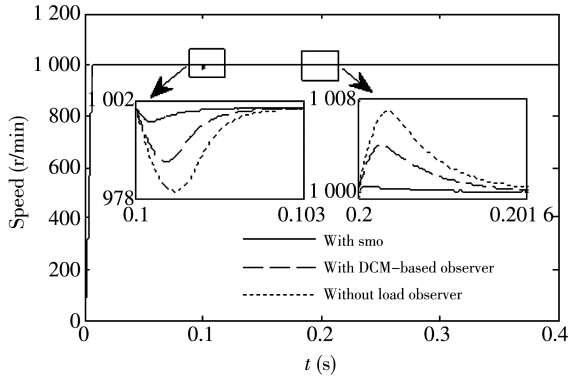

Fig. 10 Speed response with/without load observer

6 Conclusion

The FOISM-based regulator designed in this paper has better dynamic performance and improves the system's immunity to disturbances effectively. The proposed FOSMO has higher observation accuracy and faster response than the IOSMO and MRAS observers. Moreover, it also has the capability of accommodating the challenge of load disturbance superior to the other two observers. In view of the load disturbance in PMSMO control system, the designed SMO-based load observer tracks the actual load torque quickly and accurately. By introducing the observed load torque into the speed regulator, the influence of the load disturbance has been overcome effectively, thereby improving the robustness and reliability of the system.

References

[1] Lin M, Li Y H, Wu C, et al. A model reference adaptive system based sliding mode observer for model predictive controlled permanent magnet synchronous motor drive. Transactions of China Electrotechnical Society, 2017, 32 (6): 156-163.

[2] Huang J C, Li H S, Xu Q H, et al. Sensorless vector control of PMSM using sliding mode observer and fractional-order phase-locked loop. Journal of University of Science and Technology Beijing, 2012, 42 (8): 648-655.

[3] Zhu L, Wen X H, Zhao F, et al. Control policies to prevent PMSMs from losing control under field-weakening operation. Proceedings of the CSEE, 2011, 31(18): 67-72.

[4] Luo H, Wang J L, Yin Q. Low speed stability research of adaptive observer for PMSM. Electric Drive, 2013, 43 (8): 3-7.

[5] Hu Q F, Chen W Z, Qiu P F, et al. Research on fuzzy self-tuning gain PI control for accelerating and decelerating based on permanent magnet synchronous motor. Proceedings of the CSEE, 2017, 37(3): 907-914.

[6] Shi T N, Liu H, Cheng W, et al. Parameter identification of surface permanent magnet synchronous machines considering voltage-source inverter nonlinearity. Transactions of China Electrotechnical Society, 2017, 32(7): 77-83.

[7] Zhao X M, Jin H Y. Complementary sliding mode control for permanent magnet linear synchronous motor based on Elman neural network. Transactions of China Electrotechnical Society, 2018, 33(5): 973-979.

[8] Han F, Wu X D, Duan G R, et al. Attitude and orbit coupled dual sliding-mode surface control for approaching and tracking tumbling target. Transactions of China Electrotechnical Society, 2016, 31(12): 108-117.

[9] CHEN S Y, Pi Y G. Position sensorless control for permanent magnet synchronous motor based on sliding mode observer and sliding mode controller. Transactions of China Electro Technical Society, 2016, 31(12): 108-117.

[10] Dai P, Xu N, Xie H Q, et al. PMSM sliding mode control based on fast power reaching law. Electric Machines and Control, 2017, 21(11): 32-38.

[11] Wang N, Liu X Y. Load disturbance rejection based dual sliding mode control of permanent magnet synchronous motors. Journal of Dalian Maritime University, 2016, 42 (2): 75-82.

[12] Zhang B T, Pi Y G. Fractional order sliding-mode control for permanent magnet synchronous motor. Control Theory and Applications, 2012, 29(9): 1193-1197.

[13] Miao Z C, Ju M, Dang J W, et al. Speed estimation of induction motor based on fractional-order sliding-mode observer. Journal of China University of Mining and Technology, 2016, 45(6): 1256-1262.

[14] Miao Z C, Zhang H, Dang J W, et al. Design of speed controller based on A-W PI～λ for permanent magnet synchronous motors. Journal of China University of Mining and Technology, 2017, 46(4): 903-910.

[15] Zhe D D. Research of sensorless vector control for permanent synchronous motor based on sliding mode observer. Harbin: Harbin Institute of Technology, 2015.

[16] Guo W, Wang Y, Li N, et al. A speed sensorless control strategy for PMSM with model reference adaptive. Power

Electronics, 2014, 29(7): 3637-3645.
[17] Yin Z G, Zhang R F, Cao Y, et al. Research on speed estimation of permanent magnet synchronous motor based on extended Kalman filter. Journal of Power Supply, 2013, (2): 74-77.
[18] Liu H D, Zhou B, Guo H H, et al. Error analysis of high frequency pulsating signal injection method. Transactions of China Electrotechnical Society, 2015, 30(6): 38-44.
[19] Yoon Y D, Sul S K. Sensorless control for induction machines based on square-wave voltage injection. IEEE Transactions on Power Electronics, 2014, 29(7): 3637-3645.
[20] Wang C Y, Li M Q, Jiang S H. Design of fractional order control system. Beijing: National Defense Industry Press, 2014.
[21] Dadras S, Momeni H R. Fractional terminal sliding mode control design for a class of dynamical systems with uncertainty. Communications in Nonlinear Science & Numerical Simulation, 2012, 17(1): 367-377.
[22] Liu P P, Yuan X. Approximation performance analysis of oustaloup rational approximation of ideal fractance. Journal of Sichuan University (Engineering Science Edition), 2016, 48(S2): 147-154.

基于分数阶滑模观测器的 PMSM 分数阶积分滑模控制

缪仲翠，张文宾，韩天亮，余现飞

（兰州交通大学 自动化与电气工程学院，甘肃 兰州 730070）

摘　要： 针对永磁同步电机(Permanent magnet synchronous motor，PMSM)运行过程中内部参数变化和外部负载扰动影响控制性能的问题，提出了一种基于分数阶滑模观测器的 PMSM 分数阶积分滑模控制(Fractional order integral sliding mode control，FOISMC)策略。基于 FOISMC 技术，设计了分数阶积分滑模转速调节器，给出了能保证系统全局鲁棒性的全程积分滑模面设计方法。基于分数阶理论和滑模控制理论构造了分数阶滑模观测器，实现了对速度和转子位置角的高精度估计。利用滑模负载观测器对负载转矩进行了实时观测，并将观测到的负载转矩传递到转速控制器中，提高了系统抗负载扰动的能力。仿真实验验证了所提方法的可行性和有效性。

关键词： 分数阶微积分；滑模控制器；滑模观测器；无传感器控制；负载观测器；永磁同步电机

引用格式： MIAO Zhong-cui, ZHANG Wen-bin, HAN Tian-liang, et al. Fractional order integral sliding mode control for PMSM based on fractional order sliding mode observer. Journal of Measurement Science and Instrumentation, 2019, 10(4): 389-397. [doi: 10.3969/j.issn.1674-8042.2019.04.011]